Experimental Neurology 357 (2022) 114176

Contents lists available at ScienceDirect

Experimental Neurology

journal homepage: www.elsevier.com/locate/yexnr

Research paper

Characterization of non-alpha retinal ganglion cell injury responses reveals a possible block to restoring ipRGC function

John L. Hunyara [a], Sierra Foshe [a], Supraja G. Varadarajan [b], Katherine D. Gribble [a], Andrew D. Huberman [b,c], Alex L. Kolodkin [a,*]

[a] The Solomon H. Snyder Department of Neuroscience, The Johns Hopkins University School of Medicine, Baltimore, MD 21205, USA
[b] Department of Neurobiology, Stanford University, Stanford, CA 94305, USA
[c] Department of Ophthalmology, Stanford University, Stanford, CA 94305, USA

ARTICLE INFO

Keywords:
Retinal ganglion cells
ipRGCs
On DSGCs
Lin28
Axon regeneration
Intraretinal axons

ABSTRACT

Visual impairment caused by retinal ganglion cell (RGC) axon damage or degeneration affects millions of individuals throughout the world. While some progress has been made in promoting long-distance RGC axon regrowth following injury, it remains unclear whether RGC axons can properly reconnect with their central targets to restore visual function. Additionally, the regenerative capacity of many RGC subtypes remains unknown in part due to a lack of available genetic tools. Here, we use a new mouse line, *Sema6A*^{CreERT2}, that labels On direction-selective RGCs (oDSGCs) and characterize the survival and regenerative potential of these cells following optic nerve crush (ONC). In parallel, we use a previously characterized mouse line, *Opn4*^{CreERT2}, to answer these same questions for M1 intrinsically photosensitive RGCs (ipRGCs). We find that both M1 ipRGCs and oDSGCs are resilient to injury but do not display long-distance axon regrowth following Lin28a overexpression. Unexpectedly, we found that M1 ipRGC, but not oDSGC, intraretinal axons exhibit ectopic branching and are misaligned near the optic disc between one- and three-weeks following injury. Additionally, we observe that numerous ectopic presynaptic specializations associate with misguided ipRGC intraretinal axons. Taken together, these results reveal insights into the injury response of M1 ipRGCs and oDSGCs, providing a foundation for future efforts seeking to restore visual system function following injury.

1. Introduction

Optic neuropathy, due to trauma or neurodegeneration, is a leading cause of irreversible blindness worldwide. Thus far, efforts to restore function to the injured optic nerve have been unsuccessful due to the limited regeneration potential of the mammalian central nervous system (CNS) (Varadarajan et al., 2022). Encouragingly, select RGC subtypes including alpha RGCs (αRGCs), and some intrinsically photosensitive retinal ganglion cells (ipRGCs), survive up to several weeks following ONC and can regrow axons past an injury site when growth-promoting pathways are activated within these cells (Bray et al., 2019; Duan et al., 2015). However, the spectrum of differential survival and regeneration in response to various growth-promoting strategies among ~45 RGC subtypes remains poorly characterized.

Among resilient RGC subtypes, the regeneration potential of αRGCs has received the most attention since these cells are highly resilient to injury, and a knock-in mouse line (*Kcng4*^{Cre}) is available that permits genetic access to this RGC population (Duan et al., 2014; Duan et al., 2015; Krieger et al., 2017). αRGCs labeled in this line can regenerate, but this is highly dependent on the nature of prophylactic manipulations, since mTOR upregulation promotes robust axon regrowth (Duan et al., 2015) whereas overexpression of the transcription factor Sox11 compromises the survival of αRGCs but promotes regeneration of other subtypes (Norsworthy et al., 2017). For this reason, it is important to carefully characterize the survival and regeneration potential of RGC subtypes in response to a given treatment since distinct manipulations of intrinsic signaling pathways that promote axon regrowth may not lead to the same outcome in all RGC subtypes.

Much less is known about the resiliency and regenerative potential of other RGC subtypes such as ipRGCs, and also On DSGCs (oDSGCs) of the accessory optic system (AOS) (Hamilton et al., 2021). Similar to αRGCs, M1 ipRGC axons can regrow following injury, but this is highly dependent on treatment conditions. Providing a permissive environment for RGC axon regrowth with peripheral nerve grafts does not promote

* Corresponding author.
E-mail address: kolodkin@jhmi.edu (A.L. Kolodkin).

https://doi.org/10.1016/j.expneurol.2022.114176
Received 2 May 2022; Received in revised form 4 July 2022; Accepted 16 July 2022
Available online 20 July 2022

ipRGC axon re-extension following injury (Robinson and Madison, 2004), whereas overexpression of ciliary neurotrophic factor (CNTF) in RGCs promotes axon regeneration of M1 ipRGCs labeled in *Opn4*$^{CreERT2/+}$ mice (Bray et al., 2019). Only recently have genetic tools for labeling oDSGCs become available (Dhande et al., 2013; Lilley et al., 2019), thus allowing for the identification of a subpopulation of these cells as resilient to ONC (Lilley et al., 2019). However, whether the axons of these RGCs can regenerate following injury is unknown.

Recapitulating a developmental, or "pro-growth," state in injured neurons represents one approach to overcome the lack of CNS regrowth following injury. For example, activation of the RNA-binding protein Lin28, which normally functions early in development to repress the *let-7* family of microRNAs, promotes hair regrowth and digit repair following injury in adult mice (Shyh-Chang et al., 2013). Additionally, overexpression of Lin28 promotes axon regeneration of sensory neurons after sciatic nerve crush (Wang et al., 2018), of cortical spinal tract (CST) neurons following transection (Nathan et al., 2020), and of RGCs following ONC (Wang et al., 2018). Importantly, Lin28 can function cell-non-autonomously: overexpression in amacrine cells (ACs) is sufficient to promote RGC regeneration (Zhang et al., 2019). How Lin28 mediates these effects is not fully understood, although it in part involves upregulation of mTOR signaling (Nathan et al., 2020), a growth-promoting signaling pathway extensively characterized in the context of axon regeneration (Varadarajan et al., 2022).

Here, we investigate the survival and regeneration potential of the rare M1 ipRGC and oDSGC subtypes in response to Lin28a overexpression and ONC. The motivation for studying the regeneration potential of oDSGCs stems from our understanding of molecules required for connectivity of these RGCs to retinorecipient centers during development. The transmembrane semaphorin Sema6A is expressed by oDSGCs, and its binding partners plexin A2 (PlexA2) and PlexA4 are expressed in the medial terminal nucleus (MTN): PlexA2/A4–Sema6A signaling, with Sema6A serving in this context as a receptor, is required for proper oDSGC connectivity to this AOS target critical for vertical image stabilization (Sun et al., 2015). Though the molecules required for M1 ipRGCs to establish connections with the suprachiasmatic nucleus (SCN) remain unknown, the position of this ipRGC target just dorsal to the optic chiasm provides an attractive model for studying re-innervation of central targets following axon regeneration. Using genetic manipulations in the mouse to selectively assess RGC subtype regeneration following ONC, we address the survival and axon regeneration potential of these RGC subtypes. In addition to finding that M1 ipRGCS and oDSGCs are resilient to injury but do not display long-distance axon regrowth following Lin28a overexpression, we observe an unexpected response by ipRGC axons within the retina following ONC that may impact functional recovery of this circuit following injury. Taken together, these results provide novel insights into the injury response of M1 ipRGCs and oDSGCs, informing future work that seeks to restore visual system function following disease or injury.

2. Materials and methods

2.1. Animals

Opn4$^{CreERT2/+}$ mice were a gift from Dr. Samer Hattar (NIMH) (Chen et al., 2011). *C57Bl/6J* (stock number 000664) and Cre reporter *Rosa-CAG-LSL-tdTomato* (*Ai14*$^{+/-}$) (stock number 007914) mice were obtained from the Jackson Laboratory.

Sema6A$^{CreERT2/+}$ mice were generated by introducing an insert containing a RAKR furin cleavage site followed by a 2xV5 tag, a P2A linker, and the CreERT2 coding sequence into the *Sema6A* locus just downstream of exon 19 using homologous recombination embryonic stem cell technology. The targeting construct was designed, genomic organization confirmed, and function assessed by Dr. Rebecca James in the Kolodkin laboratory, and the mouse line was generated by the Janelia Gene Targeting and Transgenic Facility (James, R.E., et al., *submitted*).

The day of birth was designated as P0. Equal numbers of mice of both sexes were used in all experiments and they were housed under a 12:12 light-dark (LD) cycle. This research was carried out in strict accordance with the recommendations in the Guide for the Care and Use of Laboratory Animals of the NIH. The animal protocol was approved by the Animal Care and Use Committees of the Johns Hopkins University School of Medicine.

2.2. Immunohistochemistry

Mice were transcardially perfused with 1× PBS followed by 4% PFA in 1× PBS. All enucleated eyes were fixed in 4% PFA for 1 h at 4 °C. Dissected brains were fixed in 4% PFA overnight at 4 °C. All fixed tissue was washed several times with 1× PBS. Brains were then embedded in 3% (*w/v*) agarose and a vibratome was used to collect coronal sections at a thickness of 100 μm.

For whole mount retina and brain section staining, dissected retinas or brain sections were blocked for one hour at room temperature in 1× PBS, 0.5% Triton X-100, and 10% goat (or donkey) serum. Tissue was then incubated in primary antibody diluted in 1× PBS, 0.5% Triton X-100, and 10% goat (or donkey) serum for three days at 4 °C and washed the next day for several hours with 1× PBS, 0.5% TritonX-100 at room temperature. Tissue was incubated in secondary antibody diluted in 1× PBS, 0.5% Triton X-100, and 10% goat (or donkey) serum overnight at 4 °C and washed for several hours the next day with 1× PBS, 0.5% TritonX-100 at room temperature. Retinas or brain sections were then mounted and imaged using a Zeiss LSM 700 confocal microscope.

For retina cross-section staining, a hole was made in the cornea of fixed eyes prior to cryopreserving overnight at 4 °C in 1× PBS containing 30% sucrose (*w/v*). Cryopreserved eyes were embedded in Neg-50 frozen section medium (Richard-Allan Scientific, 6502) and sectioned using a cryostat at a thickness of 20 μm. Sections were washed three times with 1× PBS, 0.5% TritonX-100 before blocking for one hour at room temperature with 1× PBS, 0.5% Triton X-100, and 10% goat serum. Retina sections were then incubated in primary antibody diluted in 1× PBS, 0.5% Triton X-100, and 10% goat serum overnight at 4 °C and washed the next day several times with 1× PBS, 0.5% TritonX-100 at room temperature. Sections were incubated in secondary antibody diluted in 1× PBS, 0.5% Triton X-100, and 10% goat serum overnight at 4 °C and washed several times the next day with 1× PBS, 0.5% TritonX-100 at room temperature. Retina sections were then mounted and imaged with a Zeiss LSM 700 confocal microscope.

Primary antibodies used in this study include: chicken anti-GFP (Aves, GFP-1020, 1:1000), rabbit anti-melanopsin (ATS, AB-N39, 1:1000), guinea pig anti-RBPMS (PhosphoSolutions, 1832-RBPMS, 1:100), rabbit anti-dsRed (Takara, 632496, 1:1000), chicken Y-RAN RFP ((Yamagata and Sanes, 2018), 1:500, produced in Kolodkin laboratory by Dr. Randal Hand), rabbit anti-FLAG (Cell Signaling, 14793, 1:500), and guinea pig anti-vesicular acetylcholine transporter (Synaptic Systems, 139105, 1:500).

2.3. Intravitreal injections

Animals were anesthetized using isoflurane (2.5% in oxygen). A hole was made at the limbus with a 30 Gauge needle and AAV or 1 mg/ml CTβ-647 (Invitrogen, C34778) was slowly injected using a syringe (Hamilton, 7634–01). For AAV injections, 1 μl of virus was injected for all experiments except where viruses were co-injected, in which case equal volumes of virus were mixed together and 2 μl was injected. For CTβ injections, 2 μl was injected and animals were sacrificed the following day.

The following viruses were used in this study: AAV2-CAG-FLEX-tdTomato (4.8×10^{12} GC/ml; UNC Vector Core), AAV2-CMV-LacZ (7.0×10^{12} GC/ml; UNC Vector Core), AAV2-EF1α-Lin28a-FLAG (3.81×10^{12} GC/ml; Janelia Viral Tools Facility), AAV2-hSyn-FLEX-tdTomato-T2A-Syanptophysin-eGFP (2.23×10^{11} GC/ml; Salk Viral

Vector Core), AAV2-CAG-FLAG-Sema6A (2.41×10^{12} GC/ml; Janelia Viral Tools Facility).

2.4. AAV production

To generate a plasmid for AAV2-CAG-FLAG-Sema6A production, a Sema3A signal sequence (*SS*)-FLAG-Sema6A coding sequence was amplified from pCAGGS-Sema3A SS-FLAG-Sema6A (Martin Riccomagno, Kolodkin laboratory) and inserted into pAAV-CAG-GFP (Addgene 37,825) using BamH1/*Not*I sites. The resulting construct does not contain a Woodchuck Hepatitis Virus Posttranscriptional Regulatory Element sequence, however we found this is not required for FLAG-Sema6A expression in vivo. AAV2-CAG-FLAG-Sema6A virions were produced and titered by the Janelia Viral Tools Facility.

The pAAV-EF1α-Lin28a-FLAG plasmid was a gift from Xue-Wei Wang (Wang et al., 2018) and was used to produce AAV2-EF1α-Lin28a-FLAG virions at the Janelia Viral Tools Facility.

2.5. Tamoxifen injections

Tamoxifen solution was prepared by dissolving tamoxifen powder (Sigma-Aldrich, T5648) in 100% ethanol to a concentration of 80 mg/ml. Corn oil (MP Biomedicals, 901414) was added to make a working concentration of 4 mg/ml. For five consecutive days, this solution was administered via intraperitoneal injection into ≥ P42 mice at 50 mg tamoxifen/kg body weight. The mass of each animal was determined on the first day of injections and was used to calculate the volume of tamoxifen solution that was delivered over the course of the five-day treatment. Sufficient volumes of working solutions for each cohort of animals were prepared on the first day of injections and stored in the dark at 4 °C for the duration of the experiment. The same paradigm was followed for both genetic and viral labeling experiments.

2.6. Optic nerve crush

Animals were anesthetized using isoflurane (2.5% in oxygen). The left optic nerve was exposed intraorbitally and crushed with jeweler's forceps (Fine Science Tools, 11251–20, Dumont #5) for ten seconds approximately 1 mm behind the optic disc. Animals receiving sham surgery were administered the same treatment, except the optic nerve was not crushed once it was visible.

2.7. Optic nerve immunostaining

The iDISCO protocol (Renier et al., 2014) was used for staining and clearing, with slight modifications for optic nerves as described previously (Bray et al., 2017). Dissected optic nerves were dehydrated with a methanol/ddH_2O series (20%, 40%, 60%, 80%, 100%, 100%), each for 30 min at room temperature. Samples were then chilled on ice, bleached overnight with 5% H_2O_2 in 100% methanol at 4 °C, and rehydrated the next day with a methanol/ddH_2O series (80%, 60%, 40%, 20%, 1× PBS), each for 30 min at room temperature. Nerves were incubated in 1× PBS, 0.2% Triton X-100 two times for one hour at room temperature before incubating in 1× PBS, 0.2% Triton X-100, 20% DMSO, and 0.3 M glycine for two days at 37 °C. Nerves were blocked in 1× PBS, 0.2% Triton X-100, 10% DMSO, 6% goat serum for two days at 37 °C and then washed two times for one hour at room temperature with 1× PBS, 0.2% Tween 20, and 10 μg/ml heparin (PTwH). Samples were then incubated with a rabbit anti-RFP antibody (Rockland, 600–401-379, 1:1000) in PTwH, 5% DMSO, and 3% goat serum for two days at 37 °C. Nerves were washed in PTwH for 10 min, 15 min, 30 min, 1 h, 2 h, and overnight at room temperature before incubating with a goat anti-rabbit Alexa Fluor 555 antibody (Invitrogen, A21429, 1:1000) in PTwH and 3% goat serum for two days at 37 °C. The solution containing secondary antibody was syringe-filtered at 0.2 μm (Corning, 431,229) prior to use. Nerves were then washed in PTwH for 10 min, 15 min, 30 min, 1 h, 2 h, and overnight at room temperature before clearing.

2.8. Optic nerve clearing

The entire clearing procedure was performed at room temperature. Stained optic nerves were dehydrated with a methanol/ddH_2O series (20%, 40%, 60%, 80%, 100%, 100%), each for 30 min. Samples were then incubated overnight in 100% methanol before washing the next day in 66% dichloromethane and 33% methanol for three hours. Nerves were washed twice for twenty minutes in 100% dichloromethane before clearing in a 2.0 ml Eppendorf tube completely filled with 100% dibenzylether (no shaking). Cleared optic nerves were mounted onto a cover glass with dibenzylether and imaged using a Zeiss LSM 700 confocal microscope with a 20× objective (N.A. = 0.8). An optical zoom of 1.0× was used and each optical section was 1 μm. Raw images were stitched together using ZEN software (Zeiss).

2.9. RGC axon regeneration analysis

Quantification of RGC axon regeneration in the optic nerve was performed as described previously (Park et al., 2008; Wang et al., 2018). Specifically, a maximum intensity projection of every ten consecutive 1 μm thick optical slices was made to generate a series of 10 μm thick optical sections. The number of tdTomato-positive axons was counted every 250 μm past the crush site, and the nerve diameter was measured in each optical section. The number of regenerating axons per μm of nerve width was calculated and averaged over all optical sections. Σad, the total number of axons extending distance 'd' in a nerve with radius 'r', was calculated by summing over all optical sections with thickness 't' (10 μm): $\Sigma ad = \pi r^2$ x (average axons/μm)/t. Only those optic nerves for which the accompanying retinas showed evidence of widespread infectivity throughout all quadrants of the retina were included in our analyses.

2.10. Intraretinal axon orientation analysis

Each quadrant of AAV-injected *Opn4*$^{CreERT2/+}$, *Sema6A*$^{CreERT2/+}$, and *Opn4*$^{CreERT2/CreERT2}$ retinas with robust tdTomato labeling was imaged near the optic disc. A single optical section containing labeled axons was cropped to a size of 124 × 124 μm. The cropped region was chosen to avoid RGC cell bodies or tears in the retina.

All images were first processed using the smooth function in ImageJ (NIH). The dominant direction of structures, i.e. tdTomato$^+$ RGC axons, within each image was calculated using the ImageJ plug-in OrientationJ (Rezakhaniha et al., 2012), as described previously (Rosso et al., 2017). The resulting orientation coherency value is a way to characterize intraretinal axon remodeling following injury, ranging from zero (no preferential orientation of tdTomato$^+$ axons) to one (perfectly oriented tdTomato$^+$ axons).

2.11. Statistical analysis

All graphs were generated using Prism version 9 (GraphPad). Student's *t*-tests and analyses of variance (ANOVAs) were performed in Prism. The threshold for statistical significance was defined as $p < 0.05$.

3. Results

3.1. The *Sema6A*$^{CreERT2/+}$ mouse line labels oDSGCs that innervate AOS midbrain targets

Previously, we showed that a subset of MTN-innervating oDSGCs survive for several weeks following injury (Lilley et al., 2019). Since injured M1 ipRGCs also show resilience following ONC (Duan et al., 2015), we explored the full extent of oDSGC and M1 ipRGC survival and axon regeneration following injury. To study the injury response of M1

ipRGCs, we used the *Opn4*^{CreERT2} line to preferentially label M1 ipRGCs and their axons (Chen et al., 2011). Currently, the only available genetic tool to label oDSGCs of the AOS is the *Hoxd10-GFP* transgenic mouse line (Dhande et al., 2013). However, this line is challenging to use for studying oDSGC regeneration due to the presence of GFP^{+} debris within the optic nerve distal to the site of ONC, which confounds analysis of regenerating axons (data not shown). To overcome this limitation and temporally control reporter expression, we introduce here and characterize a new allele, *Sema6A*^{CreERT2}, which preferentially labels oDSGCs that comprise the AOS in adult mice.

We generated *Sema6A*$^{CreERT2/+}$*; Rosa-CAG-LSL-tdTomato*$^{+/-}$ *(Ai14*$^{+/-}$*)* animals and administered tamoxifen to characterize the extent of RGC labeling in the retina. First, we confirmed that Sema6A^{+} cells, as determined by expression of tdTomato driven by *Sema6A*^{CreERT2}, are AOS oDSGCs and do not include ipRGCs or αRGCs. We co-stained for melanopsin and observed no overlap between ipRGCs and tdTomato^{+} cells (Fig. 1A), confirming earlier observations that ipRGCs do not express Sema6A (Matsuoka et al., 2011). Importantly, we also found that *Sema6A* drives Cre expression in only ~10% of osteopontin-positive cells, a marker for αRGCs (Fig. 1B), suggesting that most αRGCs are not labeled in this line. It is also notable that many RBPMS^{-} ACs, including starburst amacrine cells, are labeled by tdTomato in *Sema6A*$^{CreERT2/+}$*; Ai14*$^{+/-}$ retinas (Fig. 1A).

Though lack of additional markers limited our ability to unequivocally determine that all oDSGCs are labeled in *Sema6A*$^{CreERT2/+}$*; Ai14*$^{+/-}$ adult retinas, we hypothesized that the subtypes of oDSGCs that innervate the MTN would be labeled by *Sema6A*^{CreERT2} since Sema6A is required in these RGCs for proper connectivity to this target during development (Sun et al., 2015). To assess whether oDSGCs were labeled in *Sema6A*$^{CreERT2/+}$*; Ai14*$^{+/-}$ retinas, we first visualized retinorecipient central targets for RGC innervation. We found that RGCs are not labeled in control *Sema6A*$^{CreERT2/+}$*; Ai14*$^{+/-}$ animals that did not receive tamoxifen (Fig. S1A). Following tamoxifen injection at P42, widespread cell body labeling indicative of Sema6A expression in *Sema6A*$^{CreERT2/+}$*;*

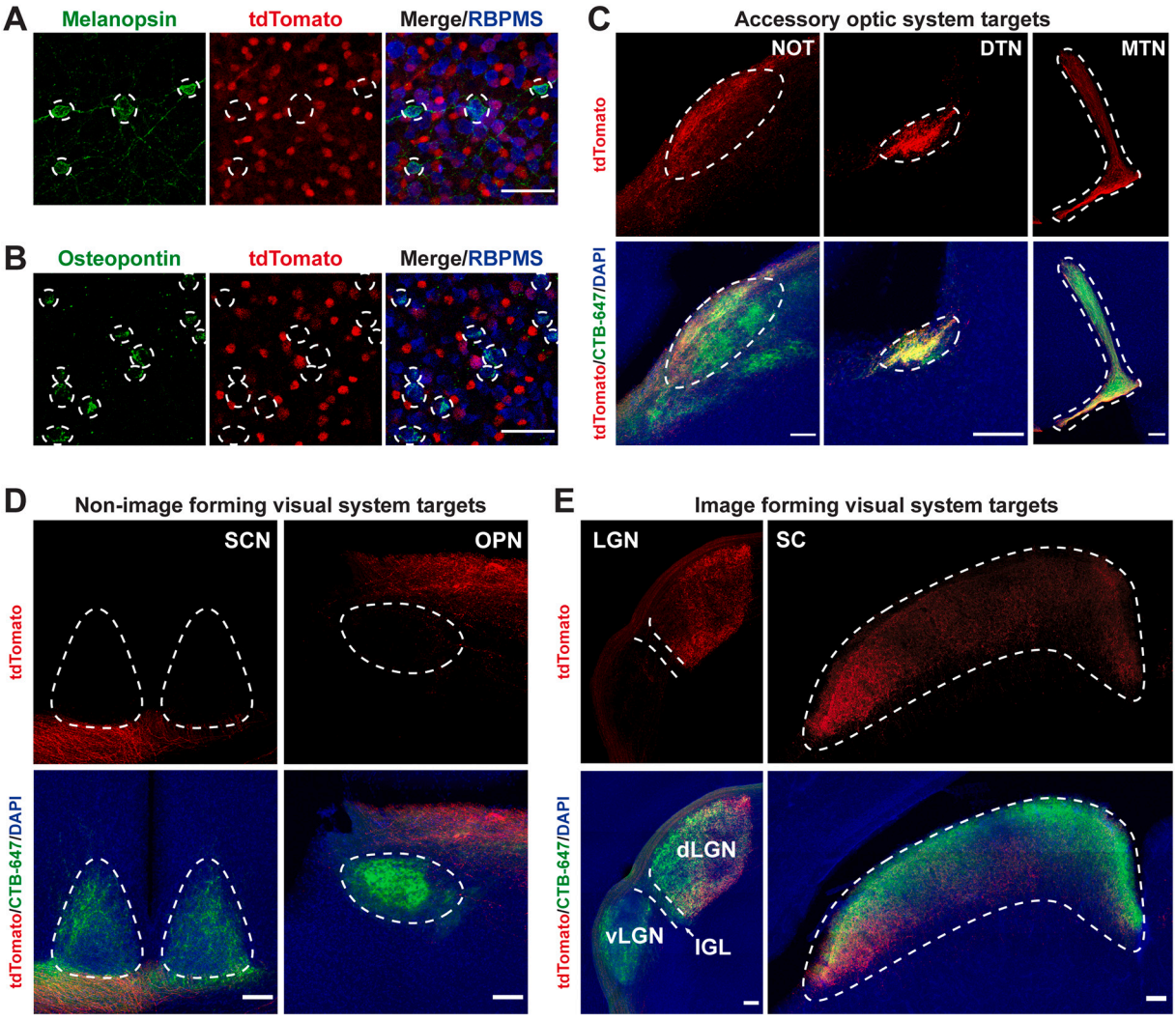

Fig. 1. oDSGCs, but not ipRGCs or αRGCs, are labeled in *Sema6A*^{CreERT2}*; Ai14*$^{+/-}$ retinas. (A) *Sema6A*$^{CreERT2/+}$*; Ai14*$^{+/-}$ adult retina co-stained with melanopsin, an ipRGC marker, and RBPMS. Melanopsin-positive RGCs are not tdTomato-positive. Dotted circles indicate melanopsin-positive cell borders. (B) *Sema6A*$^{CreERT2/+}$*; Ai14*$^{+/-}$ retina co-stained with osteopontin, an αRGC marker, and RBPMS. Osteopontin-positive RGCs are not tdTomato-positive. Dotted circles indicate osteopontin-positive cell borders. (C) RGC axon labeling in *Sema6A*$^{CreERT2/+}$*; AAV2-CAG-FLEX-tdTomato* brains following intravitreal viral injection shows strong innervation of AOS targets. Dotted white lines outline approximate target borders (from CTβ-647 signal). (D) RGC axon labeling in *Sema6A*$^{CreERT2/+}$*; AAV2-CAG-FLEX-tdTomato* brains shows no innervation of the SCN or olivary pretectal nucleus (OPN), known ipRGC central targets. Dotted white lines outline approximate target borders (from CTβ-647 signal). (E) RGC axon labeling in the brains of *Sema6A*$^{CreERT2/+}$*; AAV2-CAG-FLEX-tdTomato* mice shows some innervation of image-forming targets. Note the tdTomato-positive signal in the ventro-medial dLGN core and part of the dLGN shell; the lateral component of the SC is also innervated. An additional ipRGC target, the intergeniculate leaflet (IGL), is not innervated. Dotted white lines outline approximate target borders (from CTβ-647 signal). Scale bars = 50 μm (A,B). Scale bars = 100 μm (C-E).

Ai14$^{+/-}$ brains compromised our ability to determine whether RGC axons were innervating central targets (Fig. S1B-D). Therefore, we intravitreally injected *AAV2-CAG-FLEX-tdTomato* into *Sema6A*$^{CreERT2/+}$ adult mice and administered tamoxifen to specifically label RGCs and their central projections. This revealed robust labeling of the MTN (Fig. 1C), confirming our original expectation that MTN-innervating oDSGCs are labeled in this line. Unexpectedly, we also observed robust labeling in the nucleus of the optic tract (NOT) and the dorsal terminal nucleus (DTN) (Fig. 1C), AOS oDSGC central targets critical for horizontal image stabilization, suggesting that this line labels other AOS DSGCs and is therefore useful for studying survival and regeneration of these neurons. As expected, M1 ipRGC central targets were not labeled in this line (Fig. 1D), but we did observe that RGC axon labeling is present outside of the AOS in *Sema6A*$^{CreERT2/+}$; *AAV2-CAG-FLEX-tdTomato* brains. We observed strong labeling of the dorso-lateral and ventro-medial components of the dorsal lateral geniculate nucleus (dLGN) and also the most lateral component of the superior colliculus (SC) (Fig. 1E). This labeling could represent the ~10% of αRGCs labeled in these retinas or, possibly, On-Off DSGCs (ooDSGCs) that innervate the dLGN shell (Huberman et al., 2009). Taken together, these results show that the *Sema6A*$^{CreERT2/+}$ line labels AOS DSGCs in the adult and is a useful tool for studying the survival and regeneration of these cells following ONC.

3.2. A subset of RGCs labeled using *Sema6A*^{CreERT2} and *Opn4*^{CreERT2} mouse lines survives following ONC

In addition to *Sema6A*$^{CreERT2/+}$; *Ai14*$^{+/-}$ mice, we also generated *Opn4*$^{CreERT2/+}$; *Ai14*$^{+/-}$ mice to study the full extent of survival and regeneration in oDSGCs and M1 ipRGCs, respectively (Fig. S2A-D). To determine the long-term survival of these cell populations following injury, we performed ONC or sham surgeries in these animals and harvested retinas five weeks later. We terminated all experiments at five weeks post crush (WPC) to assess whether this is sufficient time for regenerating axons to reach central targets, an original goal of this study. We found that a subset of both *Opn4*^{CreERT2}- and *Sema6A*^{CreERT2}-labeled RGCs are present five WPC (Fig. 2A-B). >50% of labeled ipRGCs survive ONC, whereas fewer than 10% of *Sema6A*^{CreERT2}-labeled RGCs are resilient (Fig. 2C). Despite having a lower survival level, *Sema6A*^{CreERT2}-labeled RGCs represent a greater fraction of total surviving RGCs than *Opn4*^{CreERT2}-labeled RGCs (15% vs. 6%, respectively), but only because these cells constitute a larger percentage of labeled RGCs in uninjured retinas (25% vs. 1%, respectively) (Fig. 2D). These results demonstrate that a subset of both M1 ipRGCs and oDSGCs survive for several weeks following ONC, together constituting about 20% of all remaining RGCs 5 WPC.

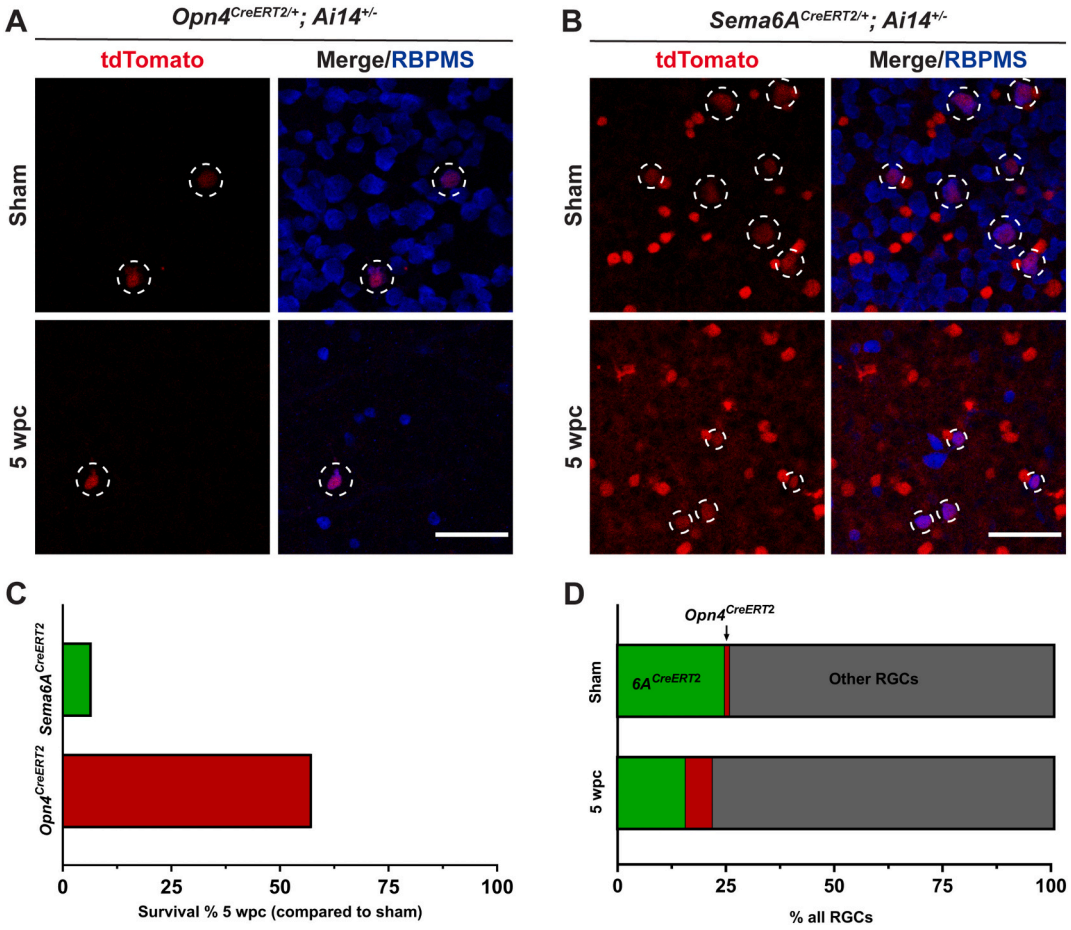

Fig. 2. *Opn4*^{CreERT2}- and *Sema6A*^{CreERT2}-labeled RGCs survive up to five weeks following injury. (A) Retinas from *Opn4*$^{CreERT2/+}$; *Ai14*$^{+/-}$ animals five weeks following either sham surgery or ONC. White dotted circles denote *Opn4*^{CreERT2}-labeled RGCs. (B) Retinas from *Sema6A*$^{CreERT2/+}$; *Ai14*$^{+/-}$ animals five weeks following either sham surgery or ONC. White dotted circles denote *Sema6A*^{CreERT2}-labeled RGCs. Remaining tdTomato-positive cells are *Sema6A*^{CreERT2}-labeled amacrine cells. (C) Percentage of labeled RGCs/retina five WPC in either *Sema6A*$^{CreERT2/+}$; *Ai14*$^{+/-}$ or *Opn4*$^{CreERT2/+}$; *Ai14*$^{+/-}$ mice compared to uninjured controls. (D) Percentage of total RGC population of *Sema6A*^{CreERT2}- or *Opn4*^{CreERT2}-labeled RGCs in uninjured animals or 5 WPC. $N = 4$ or 5 retinas per group. Scale bars = 50 μm.

3.3. Axons from RGCs labeled using Sema6A^{CreERT2}, but not Opn4^{CreERT2}, mouse lines regenerate following Lin28a overexpression

To assess subtype-specific regeneration in response to Lin28a overexpression, we initially used *Sema6A*$^{CreERT2/+}$; *Ai14*$^{+/-}$ and *Opn4*$^{CreERT2/+}$; *Ai14*$^{+/-}$ mice but found very weak axonal labeling in the optic nerve (data not shown), making it difficult to quantify the full extent of axon regeneration. Therefore, we turned to a viral labeling approach and intravitreally co-injected AAV2-*CAG-FLEX-tdTomato* with either *AAV2-CMV-LacZ* or *AAV2-EF1α-Lin28a-FLAG* two weeks prior to ONC (Fig. 3A-B). We then waited five weeks following injury to collect tissue and quantify the number of regenerating axons in the optic nerve. We observed a significant difference in the number of *Sema6A*^{CreERT2}-labeled axons that regrew 500 μm past the injury site following Lin28a overexpression (Fig. 3E-F). However, despite observing some M1 ipRGC axon regrowth up to 250 μm past the crush site, we did not find a significant degree of *Opn4*^{CreERT2}-labled axon regeneration at any distance distal to the lesion (Fig. 3C-D). Further, we did not observe any axons that regenerated the full length of the optic nerve and entered the optic chiasm in either *Opn4*$^{CreERT2/+}$ or *Sema6A*$^{CreERT2/+}$ mice (Fig. S3), consistent with previous results showing a similar degree of RGC axon regeneration in response to Lin28a overexpression (Wang et al., 2018). This suggests that efforts to promote long-distance regeneration of these RGCs will likely depend on other pro-regenerative manipulations (in the case of M1 ipRGCs) or combinatorial treatments along with Lin28a (in the case of oDSGCs) to achieve the degree of axon regrowth necessary to reach central targets following injury.

3.4. M1 ipRGC intraretinal axons are severely misguided and form ectopic branches by three weeks following optic nerve crush

To fully characterize select non-αRGC subtype responses to ONC and the effect of Lin28a on axon regeneration, we wondered whether Lin28a overexpression promotes differential survival of RGC subtypes following injury. Though this proved difficult to assess due to variability in viral infectivity from retina to retina, we did observe a striking rearrangement

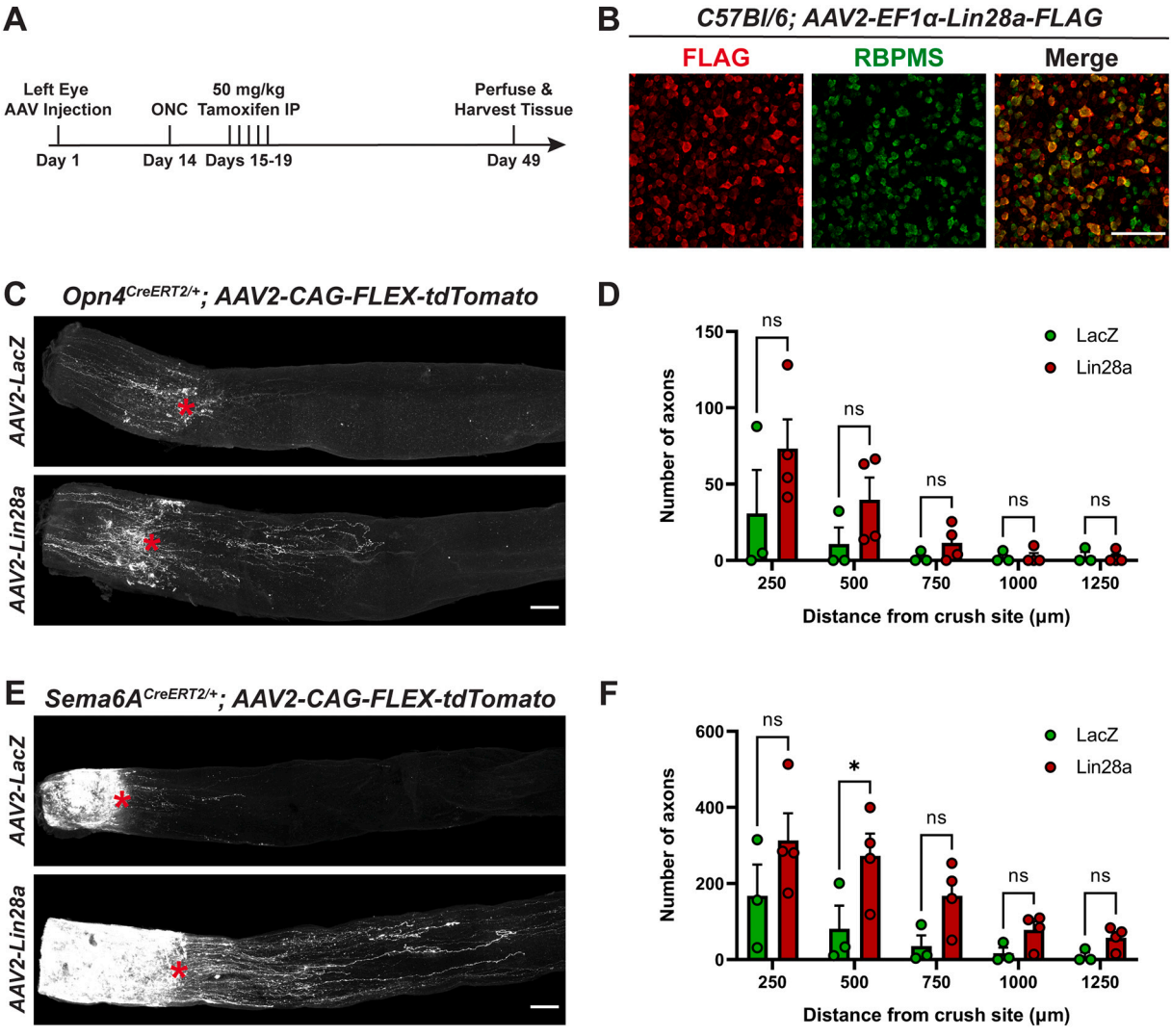

Fig. 3. Lin28a overexpression promotes axon regrowth of *Sema6A*^{CreERT2}-labeled RGCs. (A) Timeline of regeneration experiments. (B) FLAG and RBPMS staining in *C57BL/6 J* retinas injected with *AAV2-EF1α-Lin28a-FLAG*. FLAG expression is evident in the majority of RGCs. ACs in the GCL are also labeled. (C) Representative *Opn4*$^{CreERT2/+}$ optic nerves following intravitreal injection with *AAV2-CAG-FLEX-tdTomato* and either *AAV2-CMV-LacZ* or *AAV2-EF1α-Lin28a-FLAG*. Red asterisk denotes crush site. (D) Number of *Opn4*^{CreERT2}-labeled axons at indicated distances from the crush site. (E) Representative *Sema6A*$^{CreERT2/+}$ optic nerves injected with *AAV2-CAG-FLEX-tdTomato* and either *AAV2-CMV-LacZ* or *AAV2-EF1α-Lin28a-FLAG*. Red asterisk denotes crush site. (F) Number of *Sema6A*^{CreERT2}-labeled axons at indicated distances from the crush site. Statistics: two-way ANOVA, Sidak's multiple comparisons test. Bars and brackets in graphs represent mean and SEM, respectively. Symbols represent individual mice from $n = 3$ or 4 optic nerves per group. *$p < 0.05$. Scale bars = 100 μm. (For interpretation of the references to colour in this figure legend, the reader is referred to the web version of this article.)

of intraretinal *Opn4*^{CreERT2}-labeled neurites near the optic disc following ONC. Notably, this was observed in retinas infected with both *AAV2-CMV-LacZ* and *AAV2-EF1α-Lin28a*, but it was not as obvious when analyzing retinas from *Opn4*$^{CreERT2/+}$*; Ai14*$^{+/-}$ five WPC, which have much weaker dendrite and axonal labeling.

We next asked whether M1 ipRGC intraretinal axon misguidance was an ipRGC-specific injury response or if it was due AAV-mediated LacZ/Lin28a overexpression by performing ONC on *Opn4*$^{CreERT2/+}$ mice injected with only *AAV2-CAG-FLEX-tdTomato*. Since we were interested in whether this is an ipRGC-specific response, we also crushed the optic nerve of *Sema6A*$^{CreERT2/+}$ mice injected with *AAV2-CAG-FLEX-tdTomato*, since ipRGCs are not labeled in these mice. Consistent with our previous observations, we identified severely misguided neurites near the optic disc of *Opn4*$^{CreERT2/+}$*; AAV2-CAG-FLEX-tdTomato*, but not *Sema6A*$^{CreERT2/+}$*; AAV2-CAG-FLEX-tdTomato* retinas five WPC, suggesting that this is an ipRGC-specific injury response (Fig. 4A-C). This phenotype was evident in all *Opn4*$^{CreERT2/+}$*; AAV2-CAG-FLEX-tdTomato* retinas we assessed ($n = 4$) and always most pronounced near the optic disc (Fig. 4A) as compared to the retinal periphery. We determined that these tortuous neurites are likely axons based on their proximity to the optic disc and because they do not co-stain for melanopsin, which preferentially labels M1-M3 ipRGC dendrites and somas (Berson et al., 2010) (Fig. 4D). Though it has been appreciated that a subset of M1 ipRGCs survive following ONC (Robinson and Madison, 2004), this is the first report, to our knowledge, of M1 ipRGC axonal rearrangement within the retina following injury.

We next sought to learn how soon following injury ipRGC axons show defects in their radial morphology and branching within the retina. We repeated the experiment in *Opn4*$^{CreERT2/+}$ mice but harvested retinas at either one or three WPC, instead of five WPC. We observed no differences in intraretinal axon orientation one WPC (Fig. S4A,C), but by three WPC M1 ipRGC axons begin to lose their radially aligned arrangement within the retina and exhibit ectopic axon branches (Fig. S4B,D). Where labeling is sparse (Fig. S4B), it is apparent that collateral axons sprout from a subset of M1 ipRGC axons following injury, likely contributing to the misaligned orientation of these projections within the retina. This suggests that M1 ipRGC axon morphological changes, which include axon collateral formation, begin around two-three WPC and increase in complexity with time.

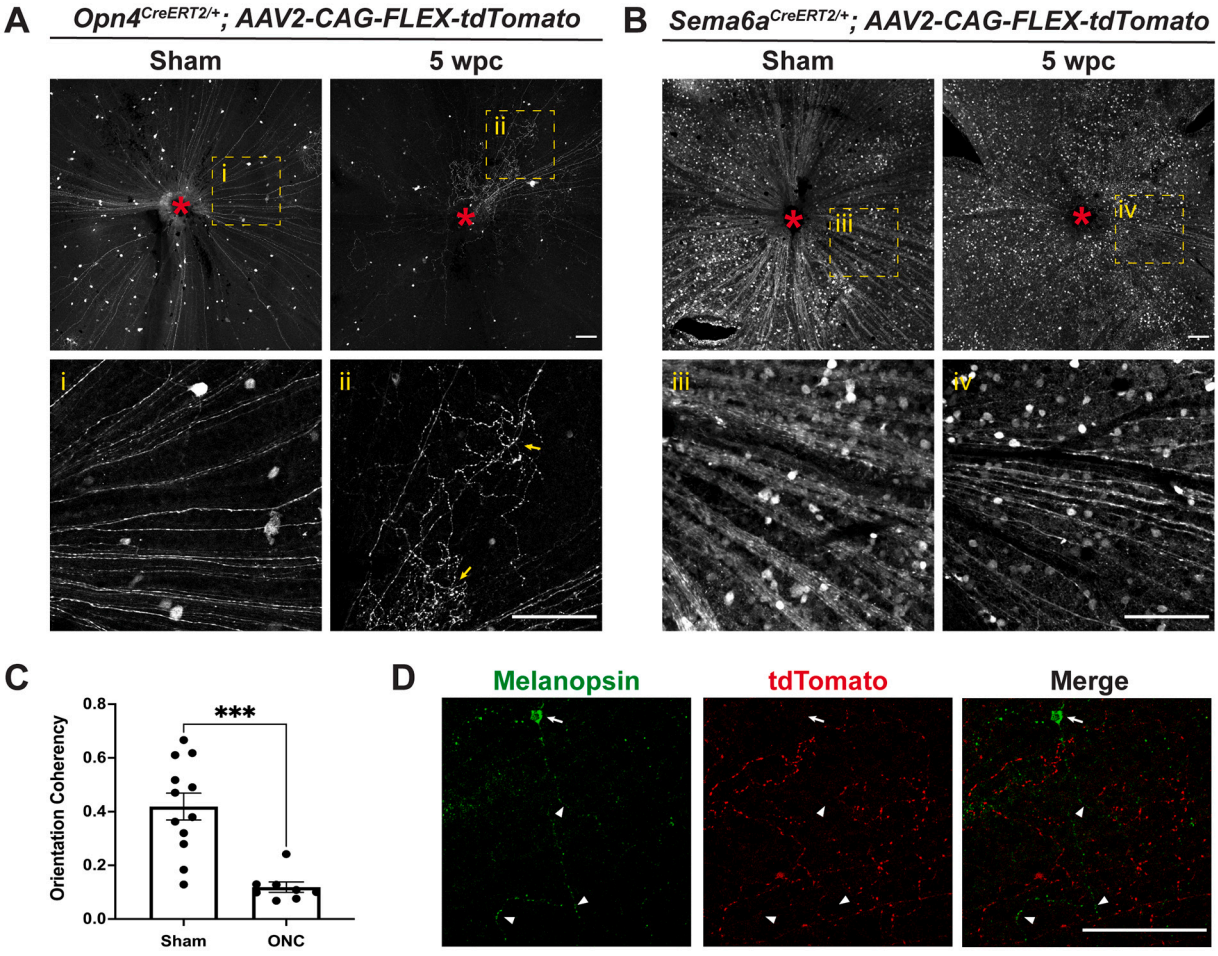

Fig. 4. *Opn4*^{CreERT2}-, but *not Sema6A*^{CreERT2}-labeled intraretinal neurites, lose their radial distribution and branch extensively five weeks post ONC. (A) Representative images of *Opn4*$^{CreERT2/+}$*; AAV2-CAG-FLEX-tdTomato* retinas five weeks following sham surgery or ONC. Yellow dotted box denotes enlarged regions shown below each panel. Red asterisk denotes optic disc. Yellow arrows indicate examples of tortuous collateral axon branches within the retina that are not radially aligned with the main axons towards the optic disc. (B) Representative images of *Sema6A*$^{CreERT2/+}$*; AAV2-CAG-FLEX-tdTomato* retinas five weeks following sham surgery or ONC. All *Sema6A*^{CreERT2}-labeled RGC axons remain radially aligned towards the optic disc at this timepoint. Yellow dotted box denotes enlarged region shown below each panel. Red asterisk denotes optic disc. (C) *Opn4*^{CreERT2}-labeled axon orientation coherency quantification (see Methods) five weeks following sham surgery or ONC. (D) Representative image of an *Opn4*$^{CreERT2/+}$*; AAV2-CAG-FLEX-tdTomato* retina 5 WPC co-stained with melanopsin. Arrow denotes melanopsin-positive soma, arrowheads indicate melanopsin-positive dendrites. Note the absence of overlap between GFP and tdTomato. Statistics: unpaired *t*-test. Bars and brackets in graph represent mean and SEM, respectively. Symbols represent individual cropped regions from $n = 3$ or 4 retinas per group. ***$p < 0.001$. Scale bars = 100 μm. (For interpretation of the references to colour in this figure legend, the reader is referred to the web version of this article.)

3.5. Ectopic presynaptic specializations are associated with misguided M1 ipRGC intraretinal axons and ectopic axon branches five weeks post-optic nerve crush

During our viral labeling experiments, we observed what appeared to be small puncta associated with *Opn4*^{CreERT2}-labeled misguided/collateral axons. Since these may be sites of contact between ipRGC axons and other cells within the retina, we next asked whether ectopic synapses are associated with M1 ipRGC axons in the retina following ONC. We injected one eye of *Opn4*$^{CreERT2/+}$ mice with the *AAV2-hSyn-FLEX-tdTomato-T2A-Synaptophysin-eGFP* virus (Oh et al., 2014), which fills Cre-expressing cells with tdTomato but exhibits GFP expression only at pre-synaptic specializations. We observed widespread GFP-positive puncta associated with tdTomato-expressing axons near the optic disc five WPC, suggesting that ectopic presynaptic specializations form within injured *Opn4*$^{CreERT2/+}$ retinas (Fig. 5B). Strikingly, only tdTomato-positive axons, but not GFP-positive puncta, were found in uninjured controls, suggesting that these synaptic contacts are a bona fide injury response (Fig. 5A). In cross sectional views of retinas from these experiments we observed that these misguided ipRGC axons typically laminate directly adjacent to the GCL within the On sublamina of the IPL, where they likely form synapses onto the dendrites of an undetermined cell type (Fig. 5C-D). Together, these findings uncover an unexpected injury response of M1 ipRGCs that may complicate efforts to restore M1 ipRGC function following injury.

3.6. M1 ipRGC intraretinal axon defects following optic nerve crush are independent of melanopsin and Sema6A

Our observations of an ONC-induced alteration of ipRGC axons within the retina motivated us to investigate molecular explanations for this phenotype and to query means to restore the radial distribution of M1 ipRGC axons following injury. First, we investigated whether melanopsin signaling underlies the formation of collateral axon branches and loss of aligned radial morphology evident in injured M1 ipRGC intraretinal axons. Melanopsin is a light responsive GPCR critical for non-image forming behaviors such as circadian photoentrainment and the pupillary light reflex (PLR). Light activation of melanopsin initiates a signaling cascade that ultimately leads to TRPC6/7 channel opening and the generation of action potentials (Xue et al., 2011). Since melanopsin signaling is unique to this RGC subtype and promotes axon growth following injury (Li et al., 2016), we generated melanopsin knockout animals (*Opn4*$^{CreERT2/CreERT2}$, (Chen et al., 2011)) and performed intravitreal viral labeling following ONC. We observed no recovery of ipRGC axon radial alignment or ectopic axon branching in melanopsin mutants five WPC compared to uninjured controls (Fig. 6A-B), suggesting that melanopsin signaling has no effect on the morphology of M1 ipRGC intraretinal axons following injury.

Finally, we explored the possibility that the axon guidance cue Sema6A influences the arrangement of intraretinal axons, since unlike M1 ipRGCs, *Sema6A*^{CreERT2}-labeled RGC axons maintain a radial orientation up to five WPC. We made an N-terminal FLAG-tagged Sema6A

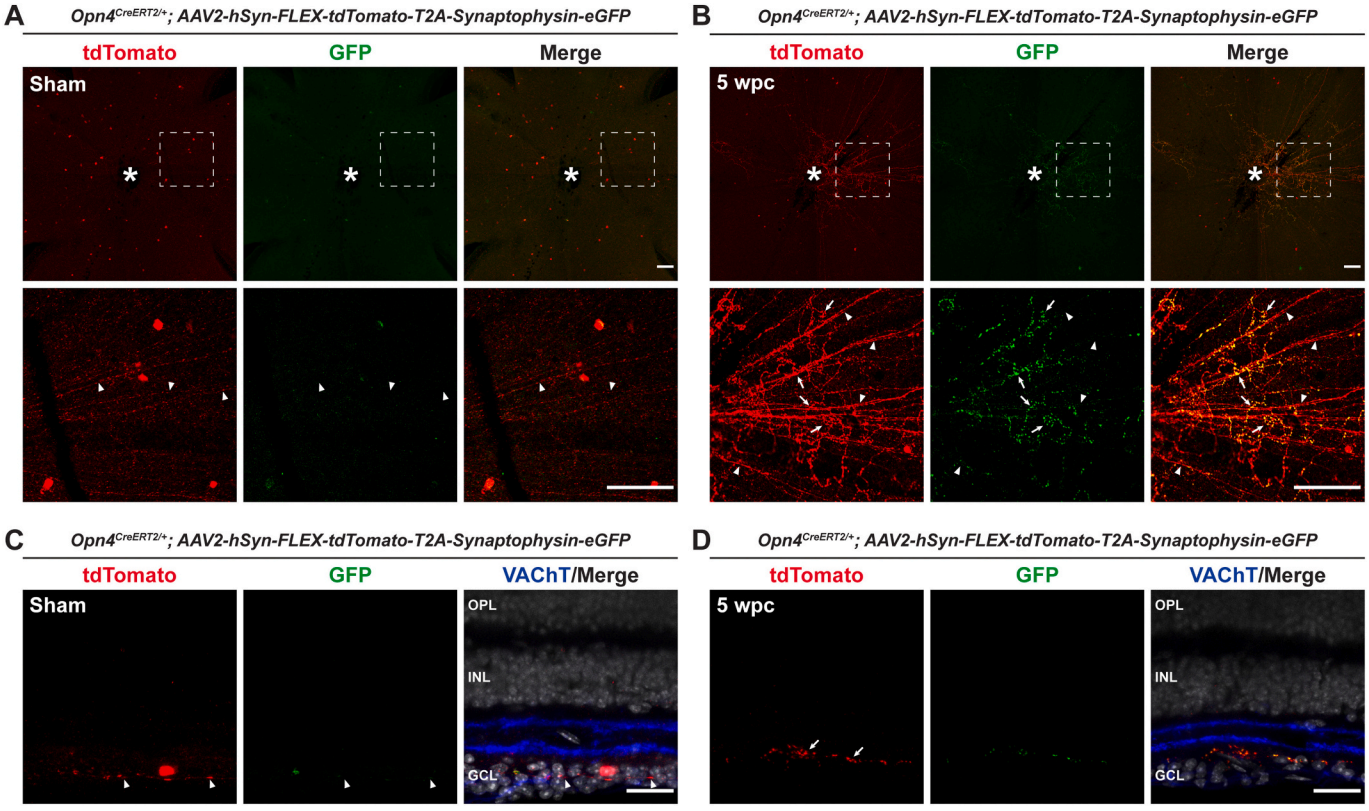

Fig. 5. Ectopic presynaptic specializations are associated with misguided *Opn4*^{CreERT2}-labeled intraretinal axons 5 weeks post ONC. (A) Representative images of *Opn4*$^{CreERT2/+}$*; AAV2-hSyn-FLEX-tdTomato-T2A-Synaptophysin-eGFP* retinas five weeks following sham surgery. White dotted box denotes enlarged region shown below. White asterisk denotes optic disc. Arrowheads indicate tdTomato-positive intraretinal axons. (B) Representative images of *Opn4*$^{CreERT2/+}$*; AAV2-hSyn-FLEX-tdTomato-T2A-Synaptophysin-eGFP* retinas five WPC. White dotted box denotes enlarged region shown below. White asterisk denotes optic disc. Arrowheads indicate tdTomato-positive intraretinal axons. Arrows indicate examples of tortuous axons and associated presynaptic specializations within the retina following ONC. (C) Cross section of an *AAV2-hSyn-FLEX-tdTomato-T2A-Synaptophysin-eGFP* retina five weeks following sham surgery. Arrowheads indicate a tdTomato-positive intraretinal axon. (D) Cross section of an *Opn4*$^{CreERT2/+}$*; AAV2-hSyn-FLEX-tdTomato-T2A-Synaptophysin-eGFP* retina five WPC showing misguided axons and associated presynaptic specializations are localized to the On sublamina of the IPL. Arrows indicate examples of tortuous axons and associated presynaptic specializations within the retina following ONC. N = 4 retinas per group. Scale bars = 100 μm (A, B). Scale bars = 25 um (C, D).

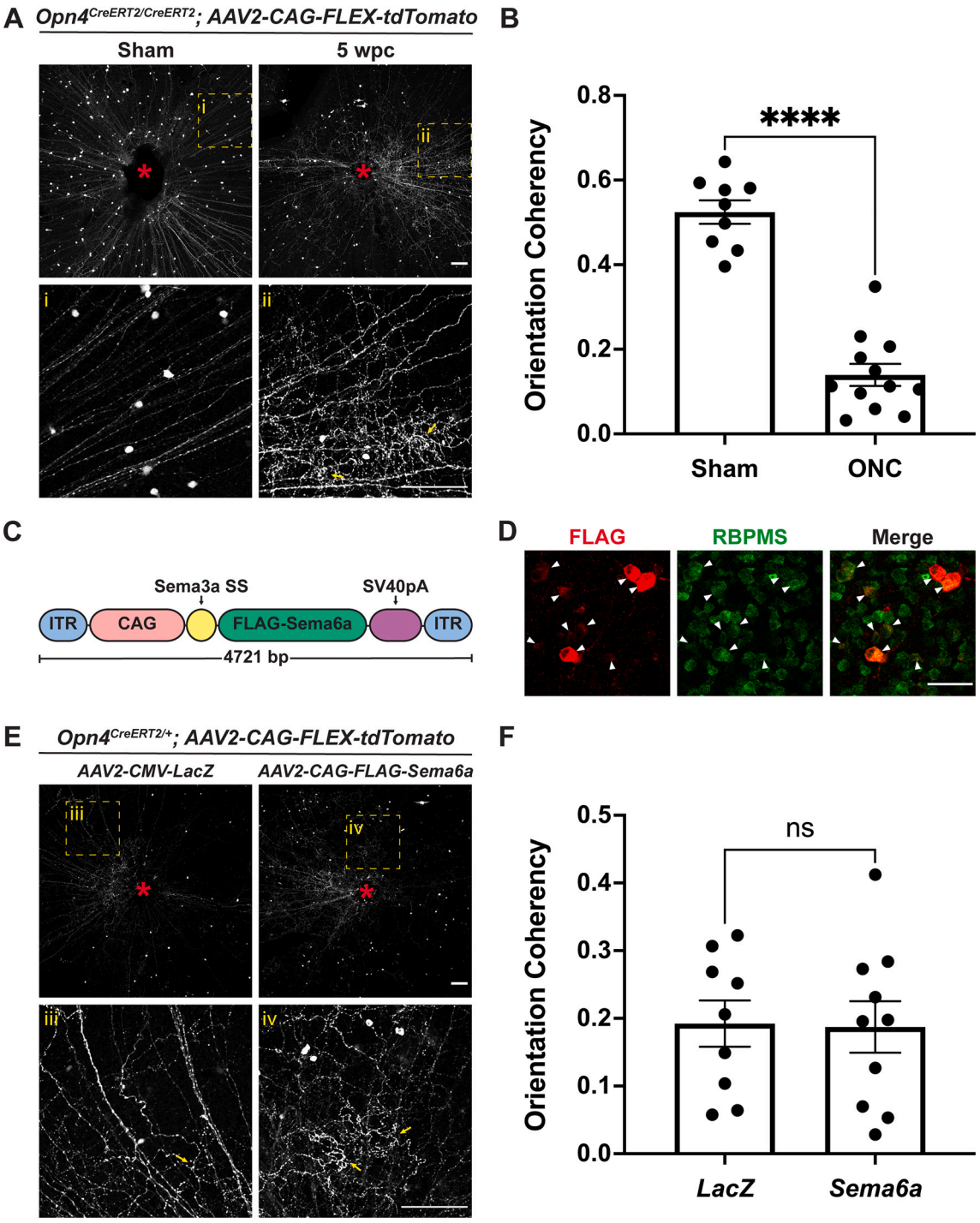

Fig. 6. Rearrangement of Opn4^{CreERT2}-labeled intraretinal axons following ONC is melanopsin- and Sema6A-independent. (A) Representative images of *Opn4$^{CreERT2/CreERT2}$; AAV2-CAG-FLEX-tdTomato* retinas five weeks following sham surgery or ONC. Yellow dotted box denotes enlarged region shown below. Red asterisk denotes optic disc. Yellow arrows indicate examples of tortuous collateral axon branches within the retina that are not radially aligned with the main axons towards the optic disc. (B) *Opn4^{CreERT2}*-labeled axon coherency quantification five weeks following sham surgery or ONC. (C) Schematic of Sema6A overexpression construct. (D) FLAG and RBPMS staining in C57BL/6 J retinas injected with *AAV2-CAG-FLAG-Sema6A*. FLAG expression is evident in RGCs (arrowheads). (E) Representative images of *Opn4$^{CreERT2/+}$; AAV2-CAG-FLEX-tdTomato* retinas five weeks following ONC. Yellow dotted box denotes enlarged region shown below. Red asterisk denotes optic disc. Yellow arrows indicate examples of tortuous collateral axon branches within the retina that are not radially aligned with the main axons towards the optic disc. (F) Opn4^{CreERT2}-positive axon coherency quantification five weeks following ONC. Statistics: unpaired t-test. Bars and brackets in graphs represent mean and SEM, respectively. Symbols represent individual cropped regions from n = 3 or 4 retinas per group. ****$p < 0.0001$. Scale bars = 100 μm (A, E). Scale bars = 50 μm (D). (For interpretation of the references to colour in this figure legend, the reader is referred to the web version of this article.)

virus for intravitreal injection and expression in RGCs (Fig. 6C). We found that FLAG-Sema6A is expressed at relatively high levels in RGCs when this virus is injected into uninjured control retinas (Fig. 6D). Therefore, we injected *AAV2-CAG-FLEX-tdTomato* into one eye of *Opn4*$^{CreERT2/+}$ mice with either *AAV2-CMV-LacZ* or *AAV2-CAG-FLAG-Sema6A* and quantified the orientation of M1 ipRGC intraretinal axons five WPC. Similar to our observations in melanopsin knockout mutants, Sema6A overexpression did not affect the alignment of intraretinal M1 ipRGC axons following injury (Fig. 6E-F). Taken together, these results suggest that melanopsin signaling and Sema6A have no effect on the orientation and collateral sprouting of M1 ipRGC intraretinal axons following optic nerve injury.

4. Discussion

Despite the inability of CNS axons to spontaneously regenerate, there are now several well-established approaches for promoting robust RGC axon regeneration within the mouse optic nerve following injury (Varadarajan et al., 2022). However, not all RGC subtypes survive and re-extend axons equally following injury (Duan et al., 2015), and distinct prophylactic manipulations can differentially affect the regenerative potential of the same RGC subtype (Norsworthy et al., 2017). Here, we build on this work and provide detailed descriptions of the survival and regenerative potential of both M1 ipRGCs and oDSGCs following ONC and Lin28a overexpression. To our knowledge, this is the first study to consider the effect of Lin28a overexpression on the regenerative potential of non αRGC subtypes. During these experiments, we also observed a novel ipRGC intraretinal axon response that occurs following ONC, thus demonstrating the importance of evaluating RGC axonal responses both distal and proximal to the crush site in order to increase the likelihood of re-establishing visual function following injury.

To study oDSGCs, we used a newly generated *Sema6A*$^{CreERT2/+}$ mouse line that labels RGCs which innervate central AOS targets: the MTN, NOT, and DTN. Importantly, we observed that very few of the other prominent resilient RGC subtypes (i.e. αRGCs and ipRGCs) are labeled in these retinas. We chose not to use the previously characterized *Pcdh9-Cre* line to study oDSGC survival and regeneration in response to Lin28a overexpression for several reasons. Previously, we observed widespread RGC labeling in *Pcdh9-Cre*$^{+/-}$*; Ai14*$^{+/-}$ retinas early in visual system development (Lilley et al., 2019), making it difficult to determine the true extent of oDSGC survival using these mice. Restricted *Pcdh9-Cre* expression in oDSGCs is observed later in life and is best visualized using intravitreal viral labeling (Lilley et al., 2019). Further, the ability to temporally control axonal tdTomato expression using CreERT2 allows for unambiguous identification of regenerating axons separate from distal axon debris that would be labeled if a virus was used to express tdTomato in oDSGC axons prior to injury.

Despite observing a dramatic loss of *Sema6A*^{CreERT2}-labeled RGCs five WPC, the surviving cells still represent approximately 15% of the entire RGC population at this timepoint. Based on our prior observations in *Pcdh9-Cre*$^{+/-}$ retinas (Lilley et al., 2019), these surviving RGCs likely include a subset of MTN-innervating oDSGCs, however, additional markers for NOT- or DTN-innervating RGCs are needed to determine the precise percentage of oDSGCs that survive following injury. Future experiments using the *Hoxd10-GFP* line, which selectively labels most all AOS DSGCs (Dhande et al., 2013), will help answer this question. We were encouraged to observe regeneration of *Sema6A*^{CreERT2}-labeled RGC axons following Lin28a overexpression, but unfortunately this does not translate into long-distance regrowth of these axons into the optic chiasm. Though Lin28a overexpression has a positive effect on *Sema6A*^{CreERT2}-labeled RGC axon regrowth, it is likely that combinatorial treatments or manipulations that alter the extrinsic environment of these regrowing axons will be required to achieve reinnervation of AOS central targets.

Our finding that approximately 50% of ipRGCs labeled in *Opn4*$^{CreERT2/+}$*; Ai14*$^{+/-}$ retinas survive five WPC was expected given that similar results for M1 ipRGCs have been previously reported (Duan et al., 2015). Our M1 ipRGC regeneration results are also consistent with the observation of modest *Opn4*^{CreERT2}-labeled axon regrowth following CNTF overexpression or PTEN deletion in ipRGCs (Bray et al., 2019). However, we did not observe significant differences in regeneration of *Opn4*^{CreERT2}-labeled axons at any distance distal to the crush site, perhaps due to the small number of axons labeled in these retinas and the highly variable degree of axon regrowth we observe within 500 μm of the injury site in control mice. Importantly, no regenerating axons were found within the optic chiasm, suggesting that M1 ipRGC axons are not among the RGC axons that have been previously shown to regrow long distances (Wang et al., 2018) and that alternative strategies should be explored to achieve functional recovery of this circuit following injury.

Unexpectedly, we also observed widespread intraretinal ipRGC axon remodeling five WPC. Initially we thought this occurred in response to Lin28a overexpression, however we found that the loss of ipRGC intraretinal axon radial morphology and the promotion of ectopic axon branching is Lin28a-independent and solely an injury-induced response. Intraretinal ipRGC axon collaterals have previously been observed in uninjured retinas, however these are relatively rare and occur in only about 7% of mouse M1 ipRGCs (Joo et al., 2013). We observe that optic nerve injury induces widespread M1 ipRGC intraretinal collateral axon formation, primarily surrounding the optic disc. Importantly, we observe that the main ipRGC axons largely remain radially aligned towards the optic disc. Therefore, the greatest contribution to the altered M1 ipRGC axon radial alignment observed following ONC is collateral axon formation. This loss of radial axon alignment and the formation of ectopic collateral axon branches is, perhaps surprisingly, melanopsin-independent, given that melanopsin overexpression promotes RGC axon re-growth following ONC (Li et al., 2016). Though intraretinal RGC axon remodeling has previously been observed following injury (Allcutt et al., 1984; Pernet et al., 2013), to our knowledge this is the first time that this injury response has been characterized as RGC subtype-specific.

We observed anatomical evidence for the formation of ectopic synapses associated with tortuous axon branches and radially mis-aligned axons within *Opn4*$^{CreERT2/+}$ retinas five WPC. Previous reports show that intraretinal ipRGC collateral axon branches are synaptically connected to dopaminergic ACs (DACs) and retrogradely signal through these cells to modulate light adaptation (Prigge et al., 2016). However, based on the position of ectopic synapses in the On sublamina of the IPL following ONC, it is highly unlikely that these contacts form onto DACs in the Off sublamina. Future efforts will determine which cell types these ectopic synapses are associated with and whether these putative connections influence retinal function.

In contrast to M1 ipRGCs, *Sema6A*^{CreERT2}-labeled axons maintain their intraretinal radial arrangement following ONC, showing that this injury response is not common to all RGC subtypes. Since Sema6A is a well-characterized axon guidance molecule, we hypothesized that this cue might control aspects of RGC axon guidance within the retina following injury, and that ectopic expression in RGCs could influence response to injury. However, we found that Sema6A misexpression in ipRGCs does not rescue the axon rearrangements observed in *Opn4*$^{CreERT2/+}$ retinas. A more thorough characterization of the M1 ipRGC transcriptome following injury is required to identify candidate genes and signaling pathways that underlie the formation of ipRGC axon collaterals in response to injury. These efforts could focus on two-three WPC, since this is when we first begin to observe alterations in the radial distribution of intraretinal ipRGC axons and the formation of ectopic axon collateral branches. Taken together, we propose that in order to provide the greatest chance of recovering ipRGC function following injury, future efforts should include not only combinatorial treatments that promote robust axon regeneration, but also manipulations that preserve normal intraretinal ipRGC connectivity. This consideration of how optic nerve injury affects intraretinal connectivity and subsequent efforts to promote visual system function may apply more generally to

other RGC types.

Supplementary data to this article can be found online at https://doi.org/10.1016/j.expneurol.2022.114176.

Declaration of Competing Interest

The authors declare no competing interest.

Acknowledgments

We are grateful to Samer Hattar for generously providing *Opn4-CreERT2* mice. We thank Nicole Kropkowski for technical assistance. We also thank Tom Johnson and members of the Kolodkin laboratory for comments on the manuscript and helpful discussions. This work was supported by the NIH (R01EY032095 to A.L.K. and A.D.·H).

References

Allcutt, D., Berry, M., Sievers, J., 1984. A qualitative comparison of the reactions of retinal ganglion cell axons to optic nerve crush in neonatal and adult mice. Brain Res. 318, 231–240.

Berson, D.M., Castrucci, A.M., Provencio, I., 2010. Morphology and mosaics of melanopsin-expressing retinal ganglion cell types in mice. J. Comp. Neurol. 518, 2405–2422.

Bray, E.R., Noga, M., Thakor, K., Wang, Y., Lemmon, V.P., Park, K.K., Tsoulfas, P., 2017. 3D visualization of individual regenerating retinal ganglion cell axons reveals surprisingly complex growth paths. eNeuro 4.

Bray, E.R., Yungher, B.J., Levay, K., Ribeiro, M., Dvoryanchikov, G., Ayupe, A.C., Thakor, K., Marks, V., Randolph, M., Danzi, M.C., et al., 2019. Thrombospondin-1 mediates axon regeneration in retinal ganglion cells. Neuron 103, 642–657 e647.

Chen, S.K., Badea, T.C., Hattar, S., 2011. Photoentrainment and pupillary light reflex are mediated by distinct populations of ipRGCs. Nature 476, 92–95.

Dhande, O.S., Estevez, M.E., Quattrochi, L.E., El-Danaf, R.N., Nguyen, P.L., Berson, D.M., Huberman, A.D., 2013. Genetic dissection of retinal inputs to brainstem nuclei controlling image stabilization. J. Neurosci. 33, 17797–17813.

Duan, X., Krishnaswamy, A., De la Huerta, I., Sanes, J.R., 2014. Type II cadherins guide assembly of a direction-selective retinal circuit. Cell 158, 793–807.

Duan, X., Qiao, M., Bei, F., Kim, I.J., He, Z., Sanes, J.R., 2015. Subtype-specific regeneration of retinal ganglion cells following axotomy: effects of osteopontin and mTOR signaling. Neuron 85, 1244–1256.

Hamilton, N.R., Scasny, A.J., Kolodkin, A.L., 2021. Development of the vertebrate retinal direction-selective circuit. Dev. Biol. 477, 273–283.

Huberman, A.D., Wei, W., Elstrott, J., Stafford, B.K., Feller, M.B., Barres, B.A., 2009. Genetic identification of an on-off direction-selective retinal ganglion cell subtype reveals a layer-specific subcortical map of posterior motion. Neuron 62, 327–334.

Joo, H.R., Peterson, B.B., Dacey, D.M., Hattar, S., Chen, S.K., 2013. Recurrent axon collaterals of intrinsically photosensitive retinal ganglion cells. Vis. Neurosci. 30, 175–182.

Krieger, B., Qiao, M., Rousso, D.L., Sanes, J.R., Meister, M., 2017. Four alpha ganglion cell types in mouse retina: function, structure, and molecular signatures. PLoS One 12, e0180091.

Li, S., Yang, C., Zhang, L., Gao, X., Wang, X., Liu, W., Wang, Y., Jiang, S., Wong, Y.H., Zhang, Y., et al., 2016. Promoting axon regeneration in the adult CNS by modulation of the melanopsin/GPCR signaling. Proc. Natl. Acad. Sci. U. S. A. 113, 1937–1942.

Lilley, B.N., Sabbah, S., Hunyara, J.L., Gribble, K.D., Al-Khindi, T., Xiong, J., Wu, Z., Berson, D.M., Kolodkin, A.L., 2019. Genetic access to neurons in the accessory optic system reveals a role for Sema6A in midbrain circuitry mediating motion perception. J. Comp. Neurol. 527, 282–296.

Matsuoka, R.L., Nguyen-Ba-Charvet, K.T., Parray, A., Badea, T.C., Chedotal, A., Kolodkin, A.L., 2011. Transmembrane semaphorin signalling controls laminar stratification in the mammalian retina. Nature 470, 259–263.

Nathan, F.M., Ohtake, Y., Wang, S., Jiang, X., Sami, A., Guo, H., Zhou, F.Q., Li, S., 2020. Upregulating Lin28a promotes axon regeneration in adult mice with optic nerve and spinal cord injury. Mol. Ther. 28, 1902–1917.

Norsworthy, M.W., Bei, F., Kawaguchi, R., Wang, Q., Tran, N.M., Li, Y., Brommer, B., Zhang, Y., Wang, C., Sanes, J.R., et al., 2017. Sox11 expression promotes regeneration of some retinal ganglion cell types but kills others. Neuron 94, 1112–1120 e1114.

Oh, S.W., Harris, J.A., Ng, L., Winslow, B., Cain, N., Mihalas, S., Wang, Q., Lau, C., Kuan, L., Henry, A.M., et al., 2014. A mesoscale connectome of the mouse brain. Nature 508, 207–214.

Park, K.K., Liu, K., Hu, Y., Smith, P.D., Wang, C., Cai, B., Xu, B., Connolly, L., Kramvis, I., Sahin, M., et al., 2008. Promoting axon regeneration in the adult CNS by modulation of the PTEN/mTOR pathway. Science 322, 963–966.

Pernet, V., Joly, S., Dalkara, D., Jordi, N., Schwarz, O., Christ, F., Schaffer, D.V., Flannery, J.G., Schwab, M.E., 2013. Long-distance axonal regeneration induced by CNTF gene transfer is impaired by axonal misguidance in the injured adult optic nerve. Neurobiol. Dis. 51, 202–213.

Prigge, C.L., Yeh, P.T., Liou, N.F., Lee, C.C., You, S.F., Liu, L.L., McNeill, D.S., Chew, K.S., Hattar, S., Chen, S.K., et al., 2016. M1 ipRGCs influence visual function through retrograde signaling in the retina. J. Neurosci. 36, 7184–7197.

Renier, N., Wu, Z., Simon, D.J., Yang, J., Ariel, P., Tessier-Lavigne, M., 2014. iDISCO: a simple, rapid method to immunolabel large tissue samples for volume imaging. Cell 159, 896–910.

Rezakhaniha, R., Agianniotis, A., Schrauwen, J.T., Griffa, A., Sage, D., Bouten, C.V., van de Vosse, F.N., Unser, M., Stergiopulos, N., 2012. Experimental investigation of collagen waviness and orientation in the arterial adventitia using confocal laser scanning microscopy. Biomech. Model. Mechanobiol. 11, 461–473.

Robinson, G.A., Madison, R.D., 2004. Axotomized mouse retinal ganglion cells containing melanopsin show enhanced survival, but not enhanced axon regrowth into a peripheral nerve graft. Vis. Res. 44, 2667–2674.

Rosso, G., Young, P., Shahin, V., 2017. Mechanosensitivity of embryonic neurites promotes their directional extension and Schwann cells progenitors migration. Cell. Physiol. Biochem. 44, 1263–1270.

Shyh-Chang, N., Zhu, H., Yvanka de Soysa, T., Shinoda, G., Seligson, M.T., Tsanov, K.M., Nguyen, L., Asara, J.M., Cantley, L.C., Daley, G.Q., 2013. Lin28 enhances tissue repair by reprogramming cellular metabolism. Cell 155, 778–792.

Sun, L.O., Brady, C.M., Cahill, H., Al-Khindi, T., Sakuta, H., Dhande, O.S., Noda, M., Huberman, A.D., Nathans, J., Kolodkin, A.L., 2015. Functional assembly of accessory optic system circuitry critical for compensatory eye movements. Neuron 86, 971–984.

Varadarajan, S.G., Hunyara, J.L., Hamilton, N.R., Kolodkin, A.L., Huberman, A.D., 2022. Central nervous system regeneration. Cell 185, 77–94.

Wang, X.W., Li, Q., Liu, C.M., Hall, P.A., Jiang, J.J., Katchis, C.D., Kang, S., Dong, B.C., Li, S., Zhou, F.Q., 2018. Lin28 signaling supports mammalian PNS and CNS axon regeneration. Cell Rep. 24, 2540–2552 e2546.

Xue, T., Do, M.T., Riccio, A., Jiang, Z., Hsieh, J., Wang, H.C., Merbs, S.L., Welsbie, D.S., Yoshioka, T., Weissgerber, P., et al., 2011. Melanopsin signalling in mammalian iris and retina. Nature 479, 67–73.

Yamagata, M., Sanes, J.R., 2018. Reporter-nanobody fusions (RANbodies) as versatile, small, sensitive immunohistochemical reagents. Proc. Natl. Acad. Sci. U. S. A. 115, 2126–2131.

Zhang, Y., Williams, P.R., Jacobi, A., Wang, C., Goel, A., Hirano, A.A., Brecha, N.C., Kerschensteiner, D., He, Z., 2019. Elevating growth factor responsiveness and axon regeneration by modulating presynaptic inputs. Neuron 103, 39–51 e35.

Update

Experimental Neurology

Volume 359, Issue , January 2023, Page

DOI: https://doi.org/10.1016/j.expneurol.2022.114256

Experimental Neurology 359 (2023) 114256

Contents lists available at ScienceDirect

Experimental Neurology

journal homepage: www.elsevier.com/locate/yexnr

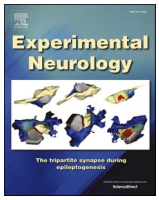

Corrigendum

Corrigendum to "Characterization of non-alpha retinal ganglion cell injury responses reveals a possible block to restoring ipRGC function"

John L. Hunyara [a], Sierra Foshe [a], Supraja G. Varadarajan [b], Katherine D. Gribble [a], Andrew D. Huberman [b,c], Alex L. Kolodkin [a,*]

[a] The Solomon H. Snyder Department of Neuroscience, The Johns Hopkins University School of Medicine, Baltimore, MD 21205, USA
[b] Department of Neurobiology, Stanford University, Stanford, CA 94305, USA
[c] Department of Ophthalmology, Stanford University, Stanford, CA 94305, USA

The authors regret that we have mistakenly cited NIH R01EY032095 for support of this work. The correct grant citation is NIH R01 **EY022713.**

The authors would like to apologise for any inconvenience this has caused.

DOI of original article: https://doi.org/10.1016/j.expneurol.2022.114176.
* Corresponding author.
E-mail address: kolodkin@jhmi.edu (A.L. Kolodkin).

https://doi.org/10.1016/j.expneurol.2022.114256

Available online 28 October 2022